Materials and Solidification

Review

Review on high-entropy alloy reinforced aluminum matrix composites fabricated by laser powder bed fusion

Hao Chen[1], Shuyu Chen[1], Gang Wang[1,✉], Dezhi Zhu[2,3,✉], Jincheng Wang[4]

Cite this article: Chen H, Chen S, Wang G, et al. *Materials and Solidification* 2026, **2**(1): 9580020. https://doi.org/10.26599/MAS.2026.9580020

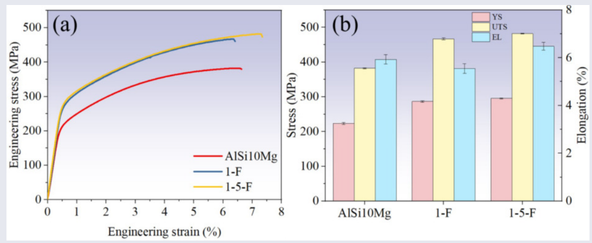

ABSTRACT: This review provides a systematic overview of the current research status and future prospects for preparing high-entropy alloy (HEA)-reinforced aluminum matrix composites (AMCs) using laser powder bed fusion (LPBF) additive manufacturing technology. Compared to conventional aluminum alloys, Al–Si-based alloys (particularly AlSi10Mg) emerge as the optimal choice for LPBF due to their narrow solidification range and excellent formability. As novel reinforcements, HEAs exhibit high strength, good plasticity, and superior deformation capability, significantly enhancing the overall performance of composites. HEAs exert grain refinement strengthening, solid solution strengthening, and dispersion strengthening effects on the Al matrix. Compared to traditional ceramic particle reinforcements, HEAs efficiently transmit loads and resist interfacial cracking, substantially reducing plasticity loss while enhancing strength. Research indicates that in HEA-reinforced AlSi10Mg composites fabricated via LPBF, HEAs exhibit excellent bonding with the aluminum matrix. A transition layer and fine secondary phases form at the interface, contributing to grain refinement. An appropriate HEA addition markedly increases the composite strength with only a slight decrease in elongation. Furthermore, synergistic effects between HEAs and other reinforcements (e.g., TiB_2) can further improve melt pool stability and optimize the material's overall performance. Although research on LPBF-fabricated HEA-reinforced AMCs remains in its infancy, it has demonstrated immense application potential. Future studies should delve deeper into the reinforcement mechanisms of HEAs in AMCs, integrating structural design and process optimization to fully leverage the advantages of additive manufacturing and advance this technology toward industrial application.

KEYWORDS: laser powder bed fusion (LPBF); high-entropy alloys (HEAs); aluminum matrix composites (AMCs); rapid solidification; mechanical properties

1 Introduction

Aluminum alloys are widely used in the aerospace, telecommunications, and automotive industries due to their high specific strength and lightweight properties [1–5]. Their affordability is also a key reason why researchers continue to explore methods for enhancing aluminum alloy strength. However, conventional aluminum alloys exhibit poor mechanical properties and wear resistance [6,7], limiting their application in critical fields. To overcome this, reinforcements (such as ceramic particles, whiskers, and fiber reinforcements) [8] or other elements (e.g., Zr [9,10], rare earths) are often added to aluminum alloys to fabricate high-performance aluminum matrix composites (AMCs). Traditional methods for producing AMCs are well established, enabling mass production while ensuring material integrity [11]. However, these conventional approaches suffer from significant drawbacks. For instance, forming individual components necessitates designing molds and forming systems [12] tailored for high-volume manufacturing. This mold-dependent production method lacks flexibility, especially for small batches where extended mold design and fabrication cycles disproportionately increase costs. Notably, the multistep nature of traditional processes introduces significant instability. The resulting AMCs often exhibit poor compatibility and wetting between reinforcements and the matrix, susceptibility to agglomeration [13,14], and a tendency for detrimental reactions at interfaces [15]. Laser powder bed fusion (LPBF) offers a superior alternative for producing higher-quality, more complex components in small batches for critical applications.

LPBF, as one of the most promising metal additive manufacturing technologies in recent years, has been widely

[1] School of Materials Science and Engineering, South China University of Technology, Guangzhou 510640, China. [2] School of Mechanical & Automotive Engineering, South China University of Technology, Guangzhou 510640, China. [3] Guangdong Key Laboratory for Advanced Metallic Materials Processing, South China University of Technology, Guangzhou 510640, China. [4] State Key Laboratory of Solidification Processing, Northwestern Polytechnical University, Xi'an 710072, China.

✉ Corresponding authors. E-mail: G. Wang, msgwang@scut.edu.cn; D. Zhu, mezhudz@scut.edu.cn

Received: December 31, 2025; Revised: March 25, 2026; Accepted: April 14, 2026

adopted for producing various high-performance complex components [16,17]. This process utilizes an ultrahigh-energy laser beam to selectively melt thin layers of powder [18]. As the molten powder rapidly solidifies during cooling and is deposited layer by layer, it generates three-dimensional (3D) parts along predetermined paths defined by computer-aided design models [19,20]. Preparing components with different structures requires only modifying the modeling, eliminating cumbersome design processes. During printing, rapid heating and cooling tendencies lead to nonequilibrium solidification, resulting in smaller grain sizes [21]. However, significant temperature gradients within the material during printing can cause coarse columnar crystals to form, degrading the material properties [22]. The quality of LPBF-printed parts depends on the process parameters, powder properties, and alloy composition [23,24]. These factors influence the behavior during melt pool solidification and the resulting microstructure, thereby affecting material performance. This also represents a significant advantage of LPBF: Material properties can be altered by adjusting process parameters. Precise parameter control enables stable production of high-quality parts with significantly reduced scrap rates. Due to the rapid solidification process of LPBF using uniformly mixed alloy powders and because each melting and solidification cycle involves an extremely small area and occurs very quickly, AMCs produced via LPBF hardly agglomerate. Harmful reactions at interfaces also lack sufficient time to occur, resulting in AMCs with higher strength. However, this process also increases the internal stress within the material after forming [25]. However, for metals with high susceptibility to thermal cracking [26], such as most aluminum alloys, cracks may form during the LPBF process. Currently, common alloys used in LPBF include titanium alloys, tool steels, and high-temperature alloys [27]. Aluminum alloys are almost exclusively eutectic or near-eutectic aluminum–silicon alloys (e.g., Al–7Si, AlSi10Mg, and Al–12Si) due to their narrow solidification range [28], which results in lower thermal cracking sensitivity.

Current research on LPBF-formed aluminum alloys primarily focuses on Alrme alloys such as AlSi10Mg. Although these alloys exhibit good formability and deliver respectable post-printing properties, they do not offer significant improvements over traditional preparation methods such as casting, particularly in terms of elongation [29,30]. Due to the high internal stresses commonly associated with additive manufacturing, the elongation of aluminum alloys formed via LPBF consistently falls far below that achieved through casting processes. Given the inherently high cost of LPBF and its inability to achieve the mass production capacity of traditional processes, the current performance of LPBF-formed aluminum alloys cannot sufficiently compensate for these limitations. To leverage LPBF's advantages, researchers are employing various methods to enhance the properties of LPBF-formed aluminum alloys, particularly aiming for a comprehensive improvement in strength and percentage elongation [31]. Researchers commonly employ elemental additions or externally added reinforcements. Elemental additions aim to generate a good reinforcing effect with the matrix but often prove difficult to control. Externally added reinforcements, however, represent a convenient, easily controllable, and highly effective method for enhancing material properties across all forming processes. The mainstream choice for externally added reinforcements is ceramic particles [32]. As the most commonly used reinforcements in AMCs, ceramic particles significantly enhance material strength and hardness. However, these hard and brittle particles often cause premature failure at the bonding interface [33,34], leading to reduced material ductility. This results in a significant trade-off: pursuing high strength typically comes at the cost of substantial ductility loss. With ongoing advancements in high-entropy alloys (HEAs), these alloys with excellent comprehensive properties have garnered increasing attention from researchers. Similar to stainless steel reinforcements, HEAs as reinforcements also hold great potential for comprehensively enhancing the mechanical properties of AMCs. HEAs inherently possess superior properties, exhibiting both higher strength and hardness than aluminum alloys [35]. As reinforcements, they can fully leverage these characteristics to significantly enhance the overall performance of AMCs. Recent studies indicate that HEAs exhibit excellent bonding with aluminum matrices and demonstrate considerable synergistic strengthening effects when combined with other reinforcements. By optimizing their content and preparation processes, the various properties of AMCs can be effectively improved, making HEAs highly promising alloy reinforcements.

This review analyzes and summarizes the formability of aluminum alloys in the LPBF process, the reinforcement effect of HEAs on aluminum alloys, and the current research status on HEA-reinforced AMCs fabricated via LPBF. It also provides an outlook for future research in this field.

2 LPBF of aluminum alloys

2.1 Formability of aluminum alloys via LPBF

Aluminum alloys used in industry are primarily categorized into eight series [36]. Among these, the 2XXX series (Al–Cu) and 7XXX series (Al–Zn) alloys, which are high-strength and heat-treatable, find the widest application in manufacturing [37–39]. Currently, 2XXX and 7XXX aluminum alloys achieve satisfactory performance through traditional manufacturing processes. Many researchers aim to leverage the advantages of additive manufacturing to significantly enhance the properties of these high-strength alloys, enabling their use in more complex components with higher service requirements. However, most aluminum alloys exhibit challenges such as wide solidification temperature ranges, high reflectivity, and susceptibility to loss of low melting point elements [40,41]. These issues often result in severe cracking and porosity defects when formed through rapid cooling in additive manufacturing [42]. Consequently, the advantages of additive manufacturing for aluminum alloys remain unrealized compared to traditional manufacturing methods. In recent years, some researchers have achieved high-density, high-performance 2XXX and 7XXX aluminum alloys through parameter optimization, the addition of reinforcements, and specialized processes. Nevertheless, the goal of significantly enhancing the properties of these alloys via additive manufacturing and achieving widespread industrial adoption remains a major challenge. To date, the most commonly produced aluminum alloys via additive manufacturing are Al–Si alloys, particularly AlSi10Mg and AlSi12 [43]. This is because Al–Si alloys generally have compositions near the eutectic point, resulting in a narrow solidification range and good fluidity.

To leverage the unique characteristics of additive manufacturing in forming processes, numerous researchers have made extensive attempts to print high-strength aluminum alloys with superior properties. Researchers first focused on optimizing printing parameters. In 2016, Zhang *et al.* [44] successfully identified a processing window for directly printing nearly fully dense 2024 aluminum alloy through parameter optimization. Their results were achieved at a high energy density of 34 $J \cdot mm^{-2}$ and a low scanning speed of 83.3 $mm \cdot s^{-1}$. By 2020 and 2021, Tan *et al.* [45] and Pekok *et al.* [46] also optimized parameters for 2024 aluminum alloy. Their findings similarly showed that the highest material density was achieved at low scan rates and high energy densities, while high scan rates resulted in extensive voids in the 2024 alloy, consistent with Zhang *et al.*'s [44] results. However, for additive manufacturing, lower scan speeds increase the processing time. Moreover, scan speed not only affects porosity but also significantly impacts microstructure and properties [47]. Lv *et al.* [48] investigated the relationship between scan speed and aluminum alloy properties while maintaining constant laser power. The results showed that tensile strength first increased and then decreased with increasing scan speed, while elongation continuously increased. This occurs because faster scanning speeds shorten the cooling process, enhancing critical internal strengthening mechanisms such as solution strengthening. However, excessively high speeds can lead to incomplete melting and other issues, introducing numerous defects that degrade material properties. Dong *et al.* [49] investigated the effect of scanning speed on the internal evolution of the aluminum alloy melt pool. They found that at high scanning speeds, the material exhibited finer grains and higher hardness. Conversely, 2024 aluminum alloy requires low scanning speeds to achieve adequate density. This approach not only increases processing time but also slows melt pool cooling, resulting in coarse grains and weakened critical strengthening mechanisms. While the resulting material may exhibit fewer defects, its performance gains remain negligible [50,51]. Therefore, while pursuing high density is undoubtedly essential for alloy material development, the ultimate focus must remain on material performance. The stringent scanning speed requirements for high-strength alloys significantly hinder their advancement in LPBF fabrication. Moreover, printing parameter optimizations for conventional alloy powders may not be applicable to composite alloy powders containing added reinforcements. Even if improvements in alloy formability are achieved, the performance of composites using such alloys as matrices cannot be guaranteed. Consequently, subsequent research has largely focused on how to print AMCs with both good formability and higher strength.

Beyond process parameters, composite powders also play a decisive role in formability and the final material properties of the formed product. To address issues such as high reflectivity and susceptibility to cracking in aluminum alloy powders [52], the addition of nucleating agents (e.g., Zr elements, ceramic particles) has proven to be an effective solution [53–55]. During additive manufacturing, fine ceramic particles or hard intermetallic compounds and solid solutions formed through reactions with the matrix act as heterogeneous nucleation sites, refining the grain size within the material [56]. Their inherent hardness also increases the composite's overall hardness and impedes dislocation movement during deformation. This enables both grain refinement strengthening and dispersion strengthening within the composite, simultaneously improving crack initiation and propagation resistance while enhancing material strength and hardness. However, powder flowability is critical for the formability of additive manufacturing materials [57]. High-strength aluminum alloys inherently exhibit poor flowability. Conventional methods of adding ceramic particles or other reinforcements to alloy powders often significantly reduce flowability during forming, ultimately resulting in numerous porosity and crack defects in the material. Therefore, the formability of any aluminum alloy is significantly influenced by the size of the reinforcement. Martin *et al.* [58] achieved crack-free selective laser melting (SLM) forming of Al7075 by uniformly adhering ZrH_2 nanoparticles to Al7075 powder via electrostatic assembly. This success primarily stems from the formation of Al_3Zr within the composite after ZrH_2 incorporation. This compound acts as a mild grain refiner, effectively reducing grain size without inducing significant crack propensity. However, it is evident that the tensile properties of Al7075 directly formed via SLM are extremely poor, as shown in Fig. 1. The crack-free forming achieved in this study was also due to the grain refinement effect of the extremely small reinforcement phase, which reduced the crack tendency. Furthermore, the dispersed nanoscale ZrH_2 did not affect powder flowability. Nevertheless, the material properties remained low, indicating that the 7075 aluminum alloy is also not suitable for additive manufacturing.

Among various aluminum alloys, Al–Si alloys, although lacking outstanding properties, exhibit superior formability compared to other aluminum alloys in the field of additive manufacturing. This characteristic allows the advantages of additive manufacturing to be effectively demonstrated during the forming process, and the direct addition of reinforcements does not significantly impair their formability. Therefore, Al–Si alloys processed via additive manufacturing can significantly enhance their properties and offer distinct application advantages, attracting keen attention from scholars in the field of additive manufacturing for aluminum alloy materials. Yang *et al.* [59] investigated the effects of process parameters on the properties of AlSi10Mg produced by LPBF. As shown in Fig. 2, at a laser power of 240 W and scan rates between 1200 and 1800 $mm \cdot s^{-1}$, the specimens exhibit favorable tensile properties and elongation. Notably, at a scan speed of 1600 $mm \cdot s^{-1}$, AlSi10Mg achieves a tensile strength of 475.18 MPa and elongation of 8.58%. For an aluminum alloy formed via additive manufacturing, this represents excellent overall performance. The fact that AlSi10Mg achieves such favorable properties solely through process control significantly reduces the time investment required for forming optimization, granting it greater development potential compared to other aluminum alloys.

For high-strength aluminum alloys, although composites obtained through specialized methods exhibit good powder formability, significant issues remain. On the one hand, while improving powder formability through complex methods is understandable, overly precise techniques substantially increase production costs for additive manufacturing, which is already an inefficient process making it suboptimal. Moreover, the resulting material properties fail to achieve a significant gap compared to traditional processes. On the other hand, the formability of high-strength aluminum alloys heavily relies on process optimization and specific additives (such as mild grain refiners). However, when seeking more effective or universal enhancement methods, formability becomes severely impacted and difficult to control.

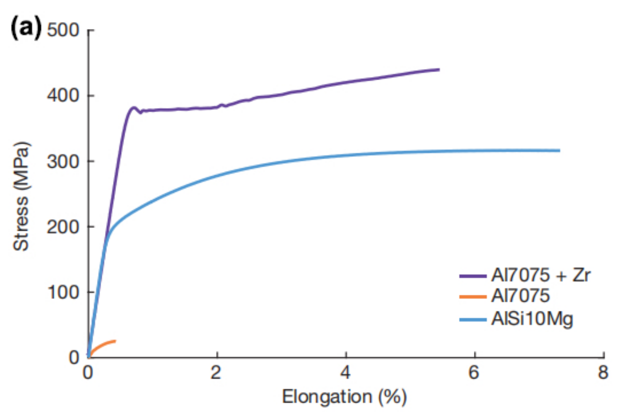

Fig. 1 Comparison of tensile properties of Al 7075 with and without Zr addition. Reproduced with permission from Ref. [58], © Macmillan Publishers Limited, part of Springer Nature 2017.

The inherent limitations of high-strength aluminum alloys constrain their advancement in LPBF manufacturing, presenting substantial challenges to this day. In contrast, Al–Si alloys such as AlSi10Mg exhibit excellent formability, eliminating the need for complex steps designed to address formability issues. This results in significantly reduced costs, and appropriate process control can directly enhance their properties. Consequently, the design approach for LPBF-fabricated alloys such as AlSi10Mg is more versatile, allowing performance enhancement through multiple avenues such as process optimization, composition control, and structural design [60]. AlSi10Mg and similar alloys are undoubtedly the optimal choice for fabricating AMCs via the LPBF process.

2.2 Selection of reinforcements in AMCs

The introduction of reinforcements in composite materials primarily occurs through two methods: exogenous addition and *in situ* generation [61]. *In situ* generated reinforcements exhibit superior bonding and compatibility with the matrix. However, for extremely fast forming processes such as LPBF, *in situ* reactions scarcely have time to occur, making exogenous reinforcements the common choice. Reinforcements can impart multiple strengthening mechanisms to composites [62], and their inherent properties also influence the performance of the composite material. As mentioned in Section 2.1, incorporating ceramic particles effectively refines the composite grain size and significantly enhances the strength. However, ceramic particles are inherently hard and brittle with minimal deformability. This characteristic leads to crack initiation at the ceramic-matrix interface under high loading conditions [63,64]. While such composites exhibit considerable strength and hardness, their brittleness increases substantially, significantly compromising plasticity. Chen *et al.* [65] investigated the effects of SiC and SiC + TiB_2 on LPBF-fabricated AlSi10Mg composites. Fracture analysis, as shown in Fig. 3, revealed that SiC_p/AlSi10Mg composites exhibited distinct brittle fracture characteristics, which transformed into brittle–ductile fracture after adding a small amount of TiB_2. This shift occurred because the TiB_2 further refined the grains, enhancing the grain refinement strengthening effect. However, numerous exposed and intact SiC particles were clearly visible on the fracture surface, indicating a weak bonding interface and inadequate load transfer from the matrix to the hard particles. Although the ceramic particles exhibit good bonding with the aluminum alloy matrix, their limited deformation capacity prevents deformation from being effectively transferred to the ceramic particles when the composite undergoes significant loading. Instead, deformation accumulates at the interface, ultimately leading to interfacial failure and compromising

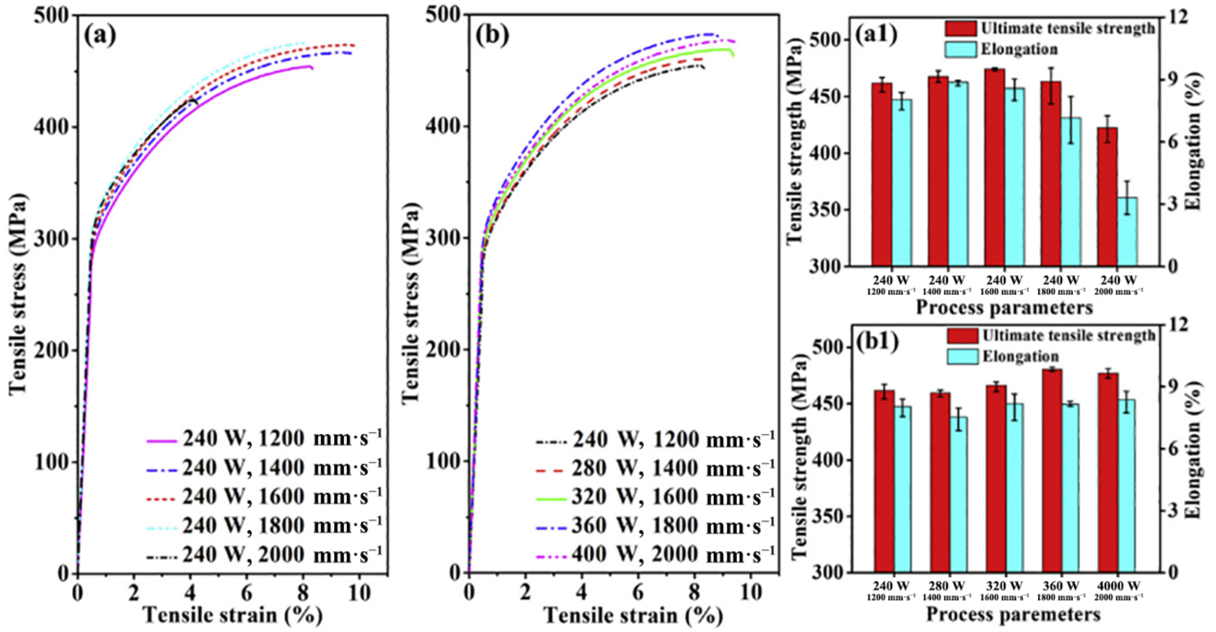

Fig. 2 Mechanical properties of AlSi10Mg under different process parameters. Reproduced with permission from Ref. [59], © Elsevier B.V. 2020.

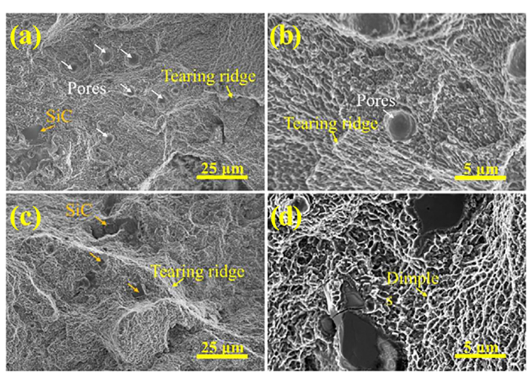

Fig. 3 Fracture morphology of composites with different constituents. (a, b) SiC_p/AlSi10Mg composite and (c, d) 1 vol% TiB_2-SiC_p/AlSi10Mg composite. Reproduced with permission from Ref. [65], © The Author(s) 2023.

composite performance. This is also a key reason why most studies on ceramic particle reinforcement have failed to achieve simultaneous enhancement of strength and percentage elongation.

Fan *et al.* [66] employed a novel electrostatic self-assembly method to prepare uniformly modified powders containing nano-TiC particles. Using the SLM process, they fabricated AlSi10Mg matrix composites. This study revealed that during SLM forming, TiC particles and the matrix *in situ* generated nucleation agent D022–Al_3Ti nanoparticles that more effectively promoted heterogeneous nucleation in the Al matrix than TiC alone. The presence of these nanoparticles resulted in ultrafine equiaxed grains within the composite that were free from cracks, significantly improving its formability. However, the study also found that a portion of TiC particles not involved in nucleation agglomerated at grain boundaries, markedly increasing intergranular brittleness and compromising the composite ductility. Thus, even nanoscale TiC particles can exert unique strengthening effects, yet they remain susceptible to agglomeration. Addressing this issue may require equipment such as ultrasonic devices [67], which correspondingly increases costs and reduces productivity.

Therefore, the bonding and compatibility between the reinforcement and the matrix must be excellent. Otherwise, the bonding interface will become a weak zone, compromising the performance of the composite material. For instance, harmful phases may form at the interface due to reactions, or low bonding strength at the interface may lead to crack initiation and propagation or even delamination of the reinforcement [68]. Additionally, to minimize plasticity loss, the reinforcement must be capable of bearing part of the deformation for the matrix, preventing rapid crack formation at the interface. This requires the reinforcement itself to possess deformation capability. Although ceramic particles are currently the most widely used reinforcement, their primary contribution to material performance enhancement stems from secondary phase strengthening and grain refinement [69,70]. Simultaneously, improving strength and ductility relies on finer ceramic particles achieving more pronounced grain refinement. Recent years have seen extensive research on nanoceramic particle reinforcement of aluminum alloys. Nanoscale particles can significantly refine grains, maximizing grain refinement strengthening and thereby improving composite ductility. However, nanoscale particles are costly to produce, prone to agglomeration during use, and difficult to control. While ceramic particles are indeed a viable choice for AMC preparation, they are far from optimal. The negative effects inherent to ceramic particles require further collaborative research and resolution.

HEAs exhibit excellent comprehensive properties, demonstrating exceptional strength and elongation after LPBF formation. In Lee *et al.*'s work [71], untreated CoCrFeNi HEAs achieved a tensile strength of 669 MPa and elongation of 38% after forming with 170 W laser power, showcasing outstanding overall material performance. Figure 4 shows the stress-strain curve of CoCrFeNi in this study. Theoretically, incorporating HEAs that possess both superior properties and good deformability into composite materials can enhance the overall performance of the composite. This approach avoids the issue of nondeformable hard particles causing cracks to readily form at interfaces. Furthermore, due to the unique properties of HEAs, the composite may experience strengthening in various aspects. The specific properties and resulting effects will be discussed in the next section.

3 HEA reinforcement through different preparation processes

3.1 Properties of HEAs

In 2004, the multicomponent alloy proposed by Cantor *et al.* [72] was officially announced and named the "Cantor" alloy. That same year, Yeh *et al.* [73] first introduced the term "HEA", defining it as a metallic alloy composed of five or more metals, each with a molar mass fraction between 5 and 35%. HEAs introduce "chemical disorder" [74] into the alloy structure by mixing multiple primary elements, forming a metallic material with high configurational entropy that predominantly tends to form a single solid solution. Due to their unique atomic arrangement, HEAs exhibit properties that are unattainable in traditional alloy systems. Their distinctive effects primarily manifest in the following four aspects: (1) High-entropy effect: Containing multiple elements, HEAs possess high mixed entropy, effectively lowering the system's free energy and enhancing stability. Within HEAs, solute and solvent elements are present in equal molar quantities and can only form single-phase solid solutions with either face-centered cubic (FCC) or body-centered cubic (BCC) structures [75]. Consequently, as single solid solutions, HEAs exhibit greater thermodynamic stability than hard, brittle intermetallic compounds, suppressing intermetallic compound formation and becoming the dominant phase. (2) Lattice distortion effect: HEAs occupy each lattice site with equal probability, yet their constituent elements exhibit size differences. Consequently, when forming solid solutions, the primary elements occupy lattice sites, inducing severe lattice distortion. The resulting stress field impedes dislocation motion, enhancing the material's strength and hardness. (3) Hysteresis diffusion effect: Interactions among HEA primary elements and the resulting lattice distortion significantly reduce diffusion rates compared to conventional alloys. This promotes stable nanophase

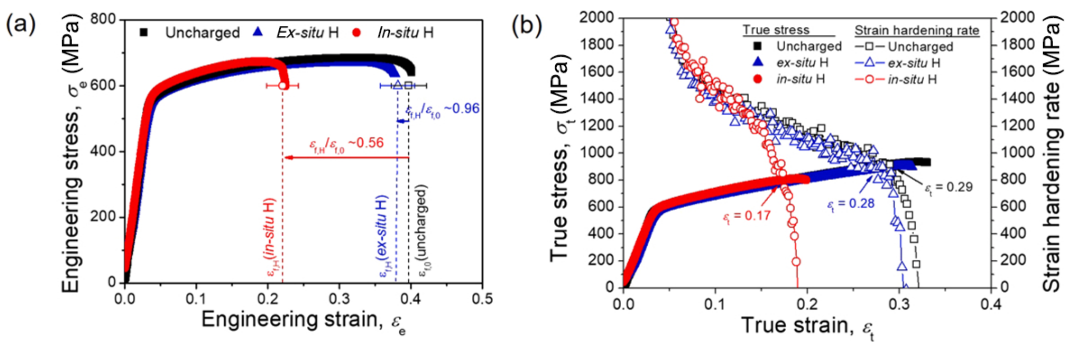

Fig. 4 LPBF-formed CoCrFeNi HEA exhibits excellent tensile properties. Specimen named "Uncharged" is directly printed CoCrFeNi. Reproduced with permission from Ref. [71], Elsevier B.V. 2023.

precipitation and slows phase transformations, helping alloys maintain stable microstructures at elevated temperatures. Consequently, the creep resistance and mechanical properties are enhanced. (4) "Cocktail" effect: The inherent properties of constituent elements and their interactions endow HEAs with complex synergistic effects unattainable by any single element. By controlling the composition and content of elements, material properties can be significantly altered. Figure 5 illustrates the above four key characteristics of HEAs [76].

3.2 Reinforcing effect of HEAs in AMCs

When micron-sized or smaller HEAs are introduced into the matrix as strengthening phases, they can refine the grain size similarly to other grain refiners. However, HEAs possess numerous unique properties, and when present in aluminum alloy matrices, their strengthening effects extend far beyond grain refinement. Jung *et al.* [77] prepared AlCoCrCuFeNi/Al composites via hot rolling. Figure 6 reveals excellent bonding between AlCoCrCuFeNi and the aluminum matrix, with intact

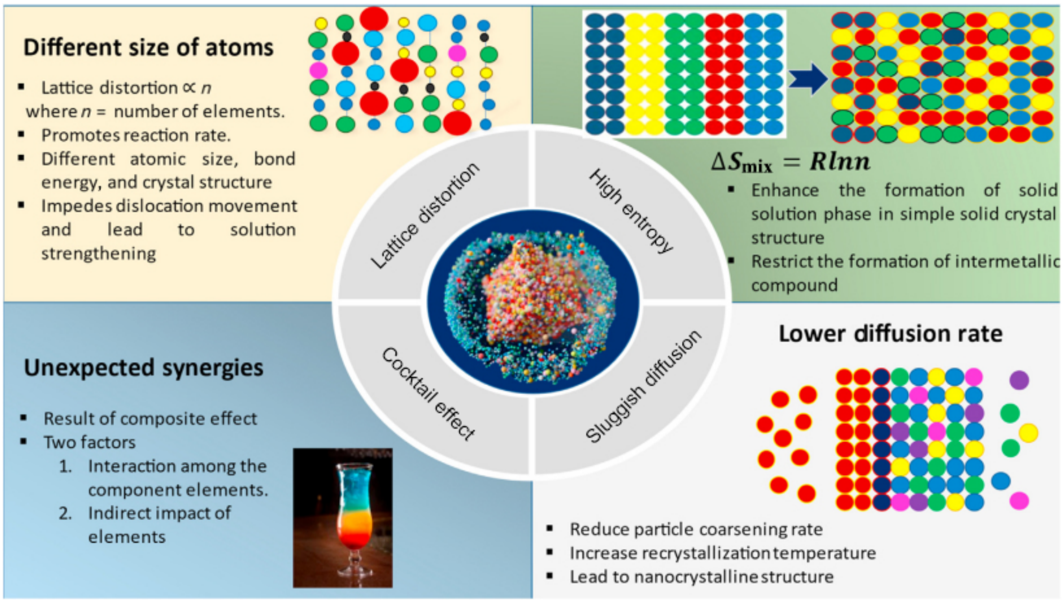

Fig. 5 Four key characteristics of HEAs. Reproduced with permission from Ref. [76], © The authors 2022.

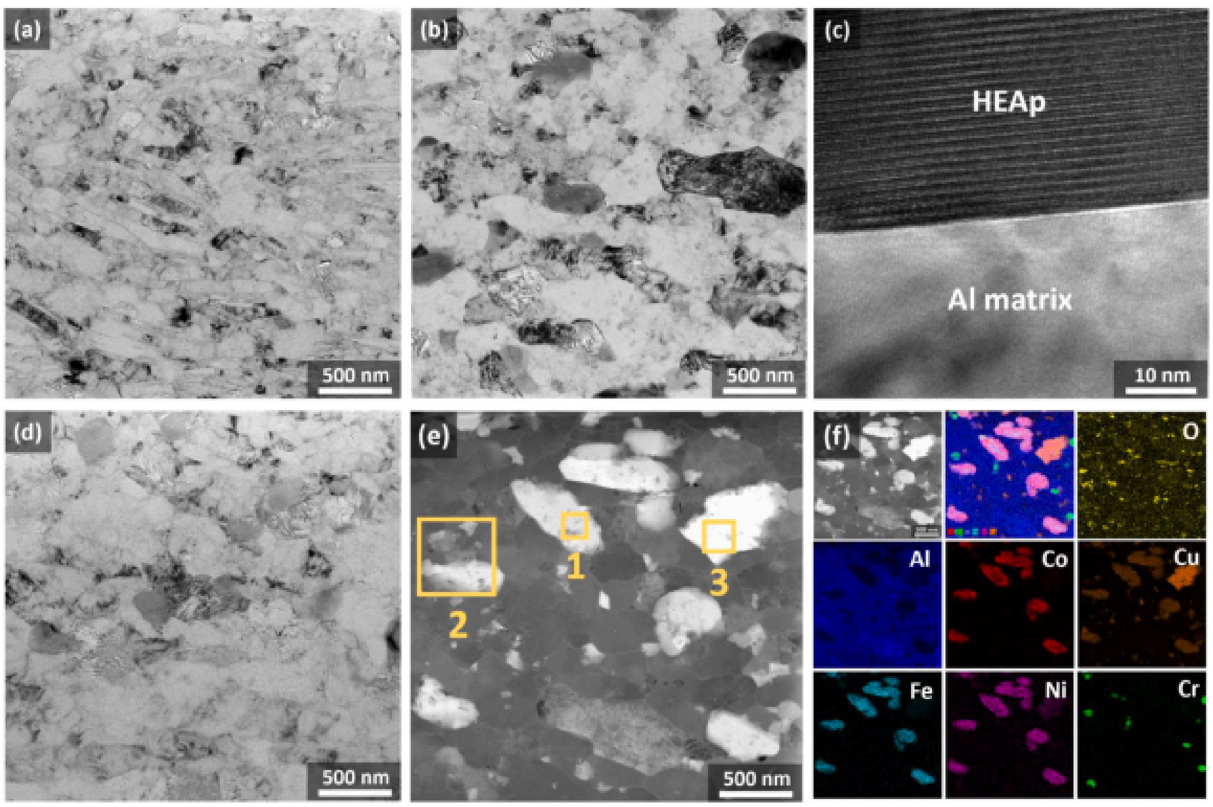

Fig. 6 (a) Pure aluminum, (b, c) HEA/Al, (d) heat-treated HEA/Al, and (e, f) their EDS analysis diagrams. Reproduced with permission from Ref. [77], © The authors 2024.

interfaces. Postheat treatment analysis showed the formation of submicron-sized solid solution phases enriched with cobalt, iron, nickel, and copper. These submicron second phases resulted from the gradual diffusion of micron-sized HEAs into the matrix. The tensile test results shown in Fig. 7 demonstrate that compared to pure aluminum produced by the same process, the composite exhibits significantly increased yield strength and fracture elongation. After heat treatment, the yield strength slightly decreases, but the fracture elongation increases substantially. This is attributed to the solid solution strengthening and grain refinement effects imparted by the micron-sized HEAs and their submicron solid solution diffusion products, enabling the composite to achieve remarkable synergistic enhancement in strength and ductility.

Beyond pure aluminum, researchers have investigated the effects of HEAs on various aluminum alloys. Gao *et al.* [78] prepared AMCs with a FeCoCrNiAl/7075Al matrix at different volume fractions using vacuum ball milling and vacuum hot-press sintering techniques. The results indicate that composites with high relative density can be produced by holding at 580 °C and 30 MPa for 10 min. The density and hardness of the HEA/Al composites increased with increasing HEA volume fraction, while their flexural strength and fracture percentage elongation first increased and then decreased. Huang *et al.* [79] investigated the dispersion of AlCrTiV HEA particles into molten pure aluminum and 7075 aluminum alloy using an ultrasonic disperser to prepare AMCs. The results indicate that AlCrTiV particles react with molten aluminum, forming $Al_{45}(Cr,V)_7$ and Al_3Ti intermetallic phases within the aluminum matrix. Enhanced dispersion and grain refinement significantly improve the material's mechanical properties. Yang *et al.* [80] prepared AlCoCrFeNi/5083Al AMCs via spark plasma sintering, investigating interface formation between HEA particles and the aluminum matrix, tensile properties, and fracture behavior. The results indicated significant enhancements in composite hardness and tensile strength, while reduced plasticity stemmed from the poor deformation capacity of the continuously distributed $Al_{13}(CoCrFeNi)_4$ phase at interfaces. Liu *et al.* [81] and Zhu *et al.* [82] studied spark plasma sintered AlCoCrFeNi/Al and $Al_{35}Ti_{15}Cu_{10}Mn_{20}Cr_{20}$/2024Al composites, respectively. Both studies revealed the *in situ* formation of shell-like particle structures within the composites. These shells segregated the reinforcements from the matrix, causing significant changes in composite properties. Zhu *et al.* [82] determined that shell-structured particles formed via thermal diffusion between the HEA core and the aluminum alloy matrix. Under quasistatic compression, the composite exhibited high compressive strength (594 MPa) and high strain at failure (26.7%), while under dynamic compression, it demonstrated high flow stress (602 MPa) and high strain at failure (45.3%). These properties surpass those of conventional ceramic-reinforced AMCs. It is evident that HEAs provide significant reinforcement for aluminum alloys of varying compositions through diverse preparation methods, yet notable challenges persist. On the one hand, the reaction of HEAs within the matrix is difficult to predict and control, potentially yielding effective reinforcing structures such as shell-like architectures or brittle metallic compounds. On the other hand, these studies employ relatively complex forming processes and require precise raw material handling, which is clearly disadvantageous for producing complex or large components. Although HEAs demonstrate good strengthening effects under numerous processes, their evolution during forming may differ from that of other forming methods. Observing the morphological evolution of HEAs during forming should be a prerequisite for their application in LPBF.

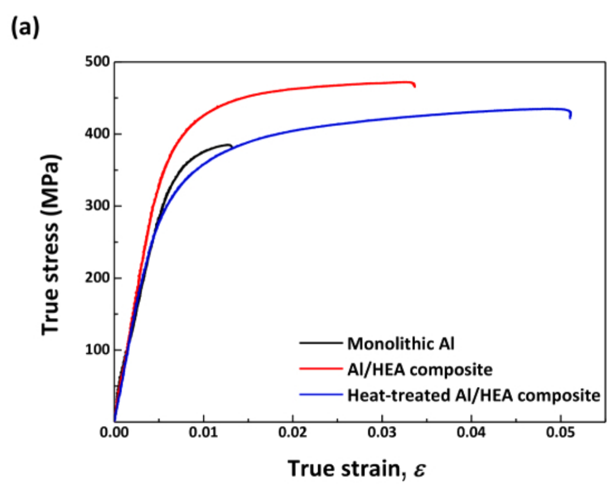

Fig. 7 True stress–strain curve of AlCoCrCuFeNi/Al composite material. Reproduced with permission from Ref. [78], ©The authors 2022.

During the preparation of composite powder, HEA particles are uniformly mixed with aluminum alloy powder through the ball milling process and are thus evenly dispersed in the powder bed. The melting point of HEAs is usually much higher than that of conventional aluminum alloys [83]. Therefore, during the laser melting process in LPBF, partially melted HEAs are deformed by the impact of molten metal in the melt pool. Under the Marangoni effect [84], the molten metal flows to fill the gaps between the dispersed HEAs. Upon solidification of the composite, HEAs remain partially molten within the microstructure, exhibiting irregular shapes [85], as shown in Fig. 8. In addition, due to the flow impact, some HEA particles have broken off, resulting in even finer particles scattered around the large particles with irregular shapes. Their behavior in the melt pool causes HEAs to concentrate near the pool boundaries. Furthermore, the impact of the molten metal on HEAs can destabilize the melt pool to some extent, thereby affecting the formability of the composite material.

From this perspective, HEAs exhibit excellent compatibility with the aluminum matrix. The complete bonding at the interface effectively enhances the joint strength, reducing the initiation of cracks at the bonding interface during material deformation. Simultaneously, the hysteretic diffusion effect of HEAs enables stable precipitation of fine secondary phases during reaction with the substrate, similar to the role of dopant elements in forming fine strengthening phases. Their inherent high strength and hardness further enhance the material strength and hardness while refining the grain size, akin to ceramic particles. Even when exhibiting irregular shapes in LPBF, their bonding with the matrix remains largely intact, although it may somewhat affect melt pool flow. Furthermore, the multielement composition of HEAs provides a reference for preparing AMCs with targeted strengthening second phases. By selecting HEAs with specific compositions based on the desired second phase, composite preparation becomes more flexible and predictable.

Furthermore, it should be pointed out that although no researchers have specifically measured the high-temperature stability of HEAs in AMCs during the LPBF process, the inherent multicomponent nature of HEAs ensures that they possess good high-temperature stability. Since LPBF involves a transient high-temperature environment and HEAs remain in a partially molten state during the process, HEAs should maintain good high-temperature stability throughout the LPBF process.

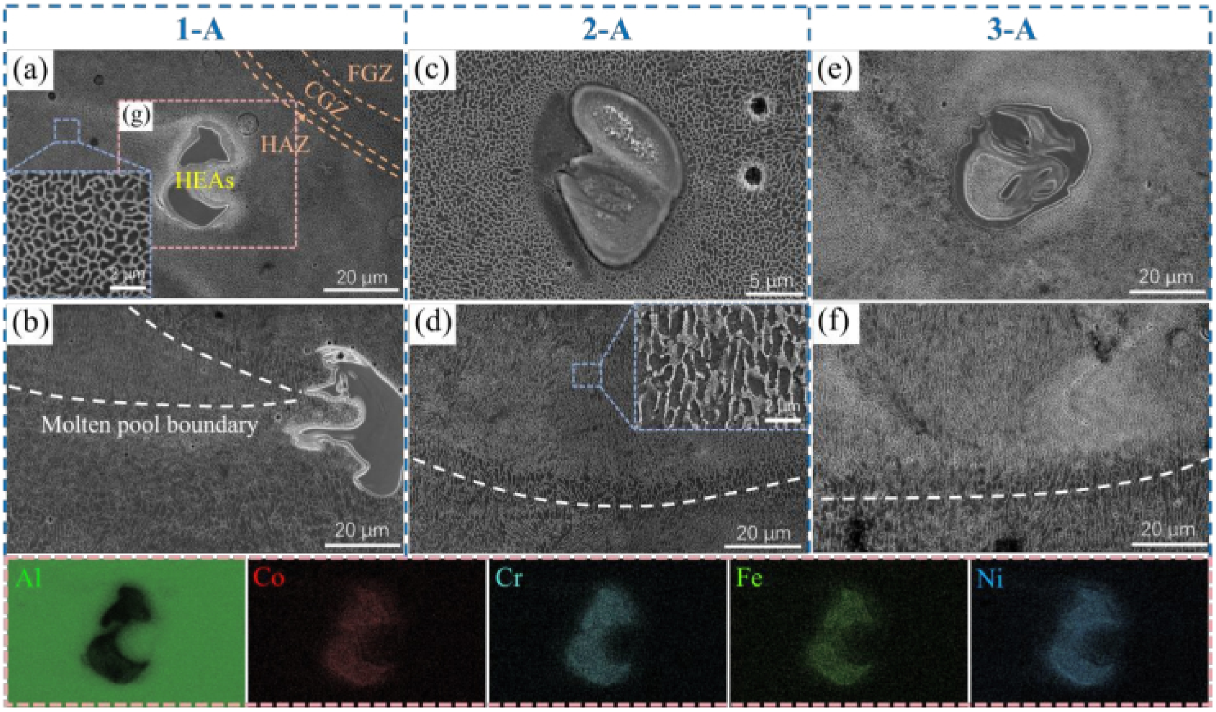

Fig. 8 Microstructure of $AlCoCrFeNi_{2.1}$/AlSi10Mg composite observed under scanning electron microscopy. Reproduced with permission from Ref. [85], © The Author(s) 2025.

3.3 Synergistic effects of HEAs with other reinforcements

To achieve significant improvements in composite material properties, adding a single reinforcement alone is often insufficient. Many researchers opt to use multiple reinforcements to enhance material performance and investigate their synergistic strengthening effects. Current studies indicate that while adding HEAs alone can simultaneously increase strength and ductility, the improvement is not substantial. Compared to other AMCs, this approach offers no clear advantage. Therefore, coadding HEAs with other reinforcements has emerged as a more promising development strategy. Li *et al.* [86] embedded silicon carbide nanoparticles within fine-grained HEA particles, forming HEA hybrid reinforcement phases enriched with nanoceramic particles. When incorporated into an Al–20Si matrix, distinct regions emerged: areas rich in nanoreinforcement and HEA phases and regions devoid of any reinforcement. Figure 9 shows the specific distribution of this inlay process within the substrate. The mixed reinforcement phase containing nanophases significantly promotes nucleation, leading to the formation of hard regions composed of fine grains and soft regions without reinforcement phases in the composite material, with distinct boundaries between the two regions. Figure 10 shows that this heterogeneous structure causes dislocations to accumulate almost exclusively in the hard regions. Due to the deformable nature of HEAs, the crack initiation and propagation facilitated by the introduced ceramic particles are significantly suppressed, thereby improving the elongation of the composite material.

Wang *et al.* [87] also combined ceramic particles with HEAs using microwave sintering technology to blend multiscale alumina micro/nanoparticles with FeCoNiCrMn HEA particles, thereby preparing a dual-phase-reinforced composite with a pure aluminum matrix. The results demonstrated that the dual-reinforced composite exhibited significantly higher yield strength, compressive strength, and hardness than AMCs reinforced solely with HEAs.

Thus, with simple design modifications, HEAs can deliver substantial strengthening effects when combined with other strengthening phases. Following the research approach outlined above, embedding ceramic particles within HEAs aims to achieve a distinct heterostructure. This integration not only addresses the tendency of nanoscale ceramic particles to agglomerate but also leverages the excellent deformation capability of HEAs. When the composite deforms under load, stress is not directly transmitted to the interface between ceramic particles and the matrix. Instead, the HEAs initially absorb part of the load and undergo deformation. HEAs, which exhibit excellent plasticity and strong bonding with the matrix, prevent direct contact between ceramic particles and the matrix. This avoids premature failure at the interface caused by accumulated deformation, theoretically improving the elongation of the composite material while paradoxically enhancing the bonding strength between ceramic particles and the matrix. This structural design approach, which fully leverages the advantages of both reinforcements while effectively mitigating the shortcomings of individual phases, is worthy of study and reference and warrants further development.

4 HEA-reinforced AMCs via LPBF

Currently, research on preparing HEA-reinforced AMCs via LPBF is scarce. On the one hand, adding trace elements and minor reinforcements to aluminum alloys or performing heat treatment after forming can yield satisfactory properties. Moreover, forming methods other than additive manufacturing can already leverage HEAs to comprehensively enhance material ductility and strength [88,89]. On the other hand, aluminum alloys generally exhibit poor laser melting formability. Addressing this formability issue is essential before considering HEA additions, limiting available research materials to primarily AlSi10Mg-based alloys. In recent years, as HEAs have gained prominence in research and additive manufacturing techniques for Al–Si alloys have matured, the integration of HEAs into additive manufacturing for aluminum alloys has become an inevitable trend.

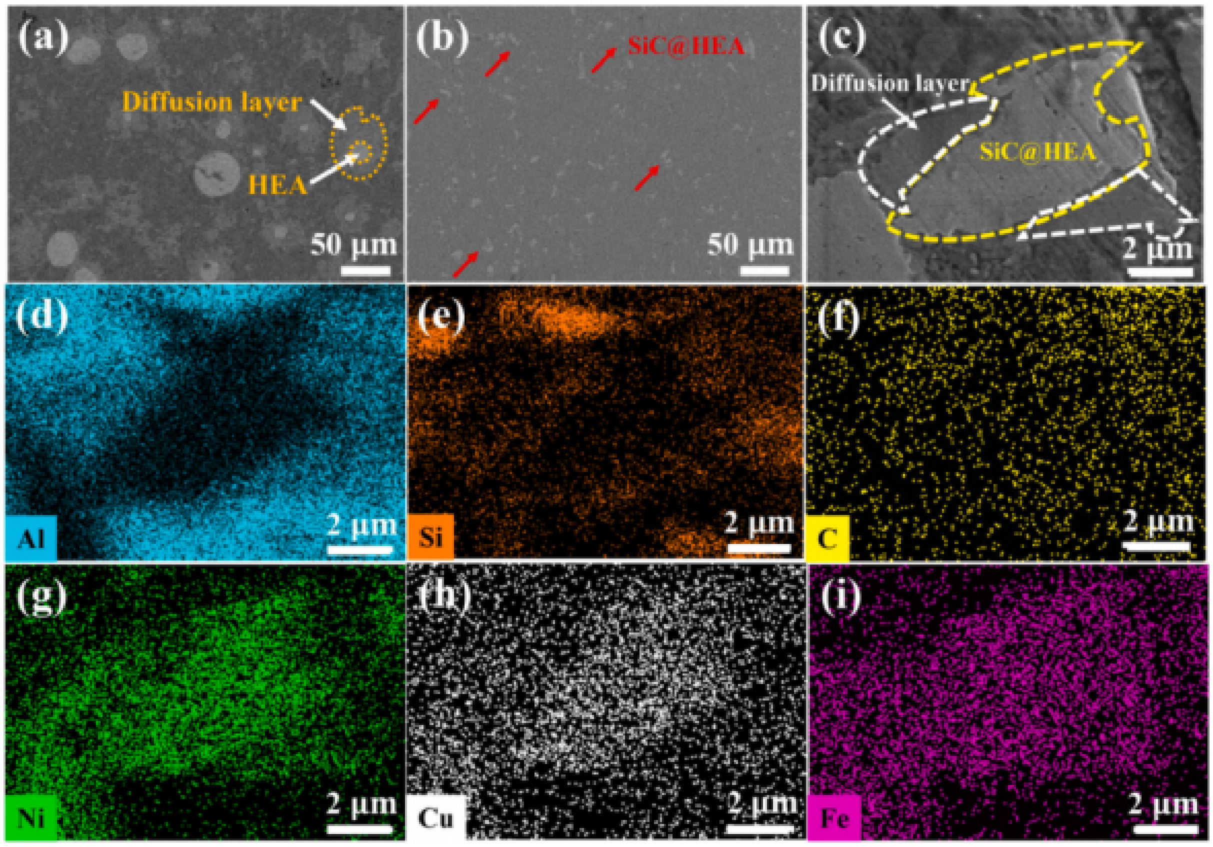

Fig. 9 Scanning electron microscopy (SEM) images of SiC@HEA/Al–20Si composite material. Reproduced with permission from Ref. [86], © Elsevier B.V. 2023.

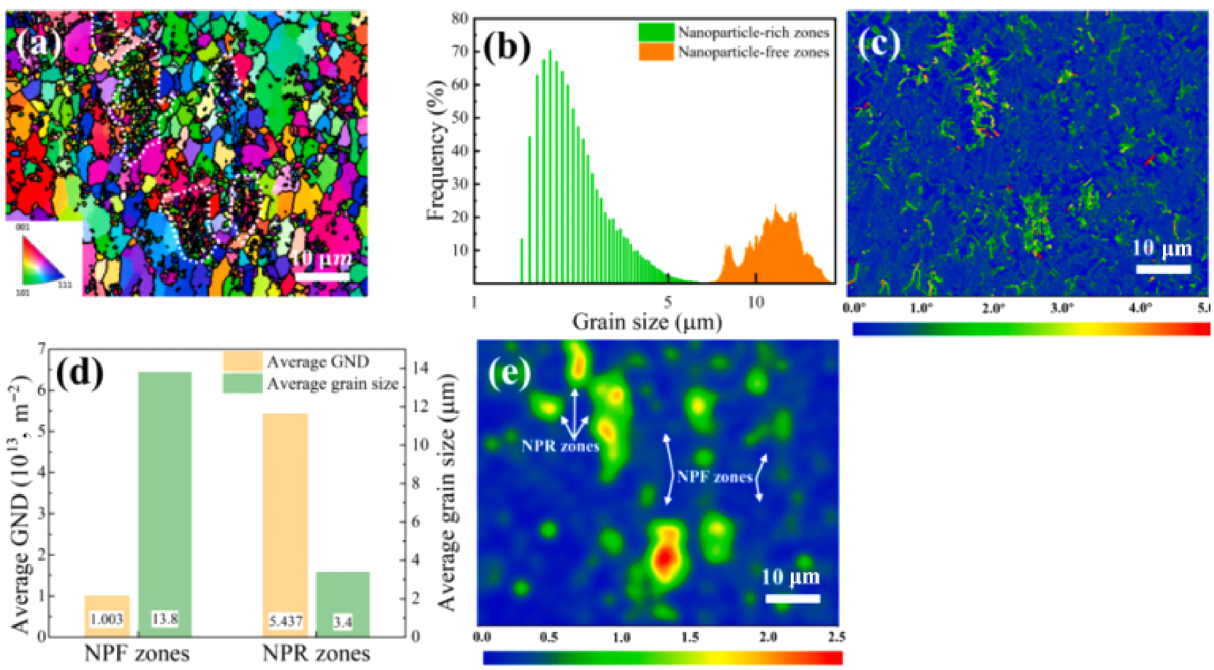

Fig. 10 Electron backscatter diffraction (EBSD) microstructure of SiC@HEA/Al–20Si composite after tensile testing. Reproduced with permission from Ref. [86], © Elsevier B.V. 2023.

Wang *et al.* [90] prepared HEA-reinforced AlSi10Mg–matrix composites containing 5 wt% $Al_{0.9}CoCrFeNi$ using the LPBF process. In the composites fabricated under three laser powers (190, 220, and 250 W), distinct transition layers were observed at the interfaces between the HEA and the matrix, accompanied by well-dispersed σ phases enriched in Fe and Cr, as shown in Fig. 11. The σ phase, formed by the diffusion of HEAs into the matrix, provided abundant nucleation sites, significantly refining the grain structure. However, as shown in Fig. 12, the brittle metallic compound σ phase resulted in a significant decrease in elongation compared to the AlSi10Mg alloy. Despite this, the tensile properties of the composites prepared in this study still

清華大学出版社 Tsinghua University Press | SciOpen

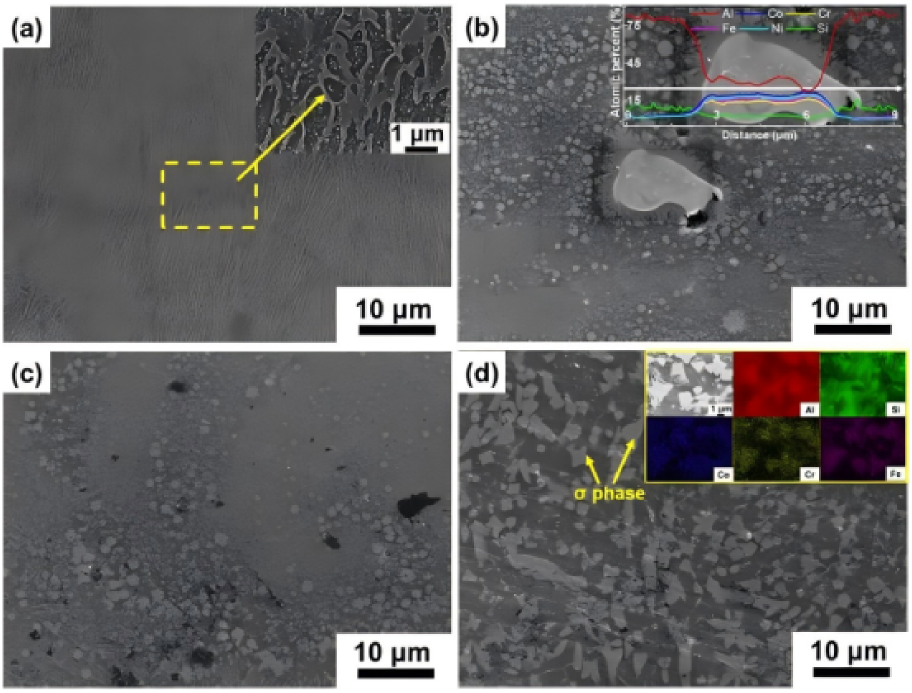

Fig. 11 SEM images of AlSi10Mg composite reinforced with $Al_{0.9}CoCrFeNi$ HEA. Reproduced with permission from Ref. [90], © Elsevier B.V. 2021

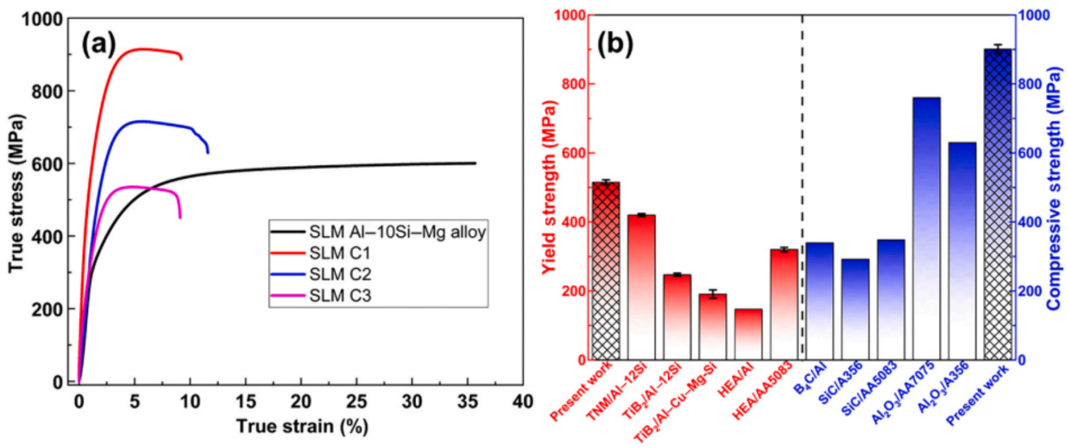

Fig. 12 Performance comparison of AlSi10Mg and other materials enhanced by $Al_{0.9}CoCrFeNi$ HEA. Reproduced with permission from Ref. [90], © Elsevier B.V. 2021

demonstrated a clear advantage over results from other studies using different materials.

Chen [85] prepared AlSi10Mg composites reinforced with $AlCoCrFeNi_{2.1}$ HEA and (TiB_2 + $AlCoCrFeNi_{2.1}$)/AlSi10Mg composites via LPBF. Unlike Wang *et al.*'s study [90], Chen's research [85] did not reveal any obvious intermetallic compounds; instead, only faint traces of nanoscale particles were observed in the transition layer at the interface. It remains unclear whether these particles are the result of diffusion or tiny fragments of HEAs dispersed by the molten metal, which need to be investigated further. The results indicate that incorporating $AlCoCrFeNi_{2.1}$ significantly enhances both the tensile strength and yield strength of the composites, although elongation decreases. This is primarily attributed to the introduction of additional voids during $AlCoCrFeNi_{2.1}$ addition, with porosity increasing alongside higher $AlCoCrFeNi_{2.1}$ content, as shown in Fig. 13. The incorporation of HEAs may exacerbate melt pool instability during LPBF formation.

The addition of TiB_2 to the composite material significantly decreased its porosity. Notably, the TiB_2 content in our study ranged from only 0.05 to 0.15 wt%, indicating that a moderate amount of TiB_2 can reduce the instability of the composite material, as shown in Fig. 14. Generally, the addition of TiB_2 tends to reduce ductility; however, in this study, ductility was actually enhanced. Such a small amount of TiB_2 undoubtedly exerts only a negligible grain refinement effect, indicating that the primary cause of grain refinement in the composite is the introduction of HEAs. The minimal TiB_2 serves to stabilize the molten pool, allowing the advantages of HEAs to be fully realized. The fracture analysis shown in Fig. 15 reveals that $AlCoCrFeNi_{2.1}$ exhibits good bonding with the matrix, with a fracture mode characterized as ductile-brittle fracture. Secondary cracks appeared on some $AlCoCrFeNi_{2.1}$ particles, indicating that the load was effectively transferred to the $AlCoCrFeNi_{2.1}$ particles, thereby mitigating the impact of the reinforcement addition on plasticity.

Chen [85] also prepared FeCoCrNi/AlSi10Mg composites via LPBF. Compared to $AlCoCrFeNi_{2.1}$, FeCoCrNi exhibited markedly different effects on composite formation. As shown in Fig. 16, the porosity of the FeCoCrNi/AlSi10Mg composites was lower than that of AlSi10Mg, indicating that FeCoCrNi enhanced the melt pool stability. As evident from Fig. 17, the introduction of 1 wt% FeCoCrNi substantially increased the tensile strength of the composite with minimal sacrifice in elongation. Although the tensile strength of this composite did not surpass that of $AlCoCrFeNi_{2.1}$/AlSi10Mg, FeCoCrNi clearly demonstrated superior advantages in enhancing the overall performance. Moreover, after adding trace amounts of TiB_2 particles, the composite material demonstrated significant improvements in both ductility and strength compared to AlSi10Mg, achieving synergistic enhancement of strength and percentage elongation in AMCs fabricated via LPBF.

Currently, research on LPBF-fabricated HEA-reinforced AMCs remains limited. However, existing studies indicate that HEAs offer distinct advantages over other reinforcements, such as ceramic particles. The incorporation of HEAs enhances strength while mitigating the negative impact of reinforcing particles on

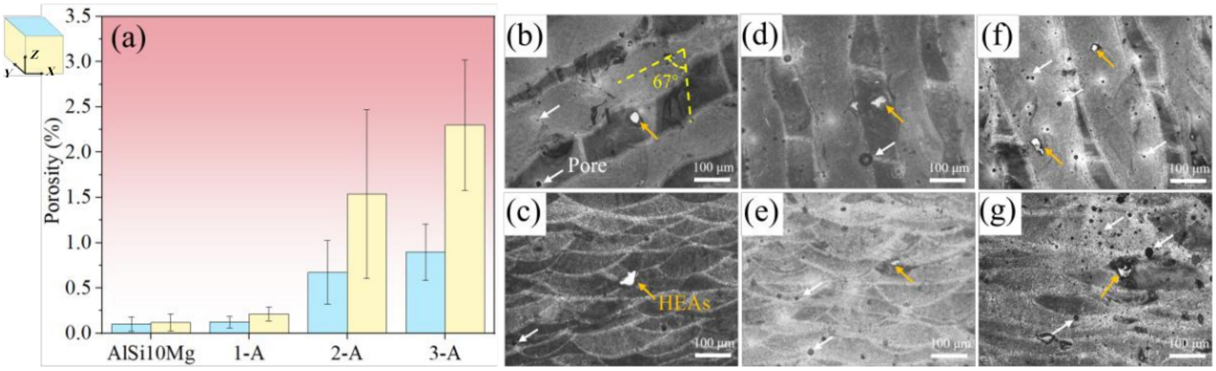

Fig. 13 $AlCoCrFeNi_{2.1}$/AlSi10Mg porosity statistics. Reproduced with permission from Ref. [85], © The Author(s) 2025.

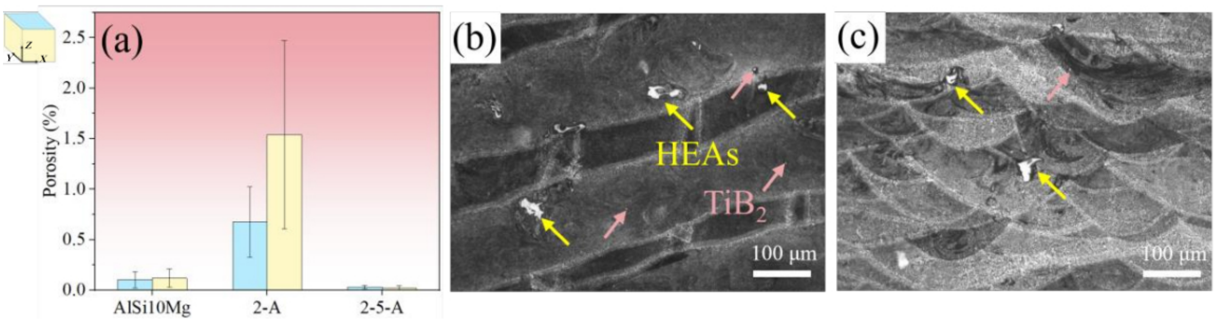

Fig. 14 (TiB_2 + $AlCoCrFeNi_{2.1}$)/AlSi10Mg porosity statistics. Reproduced with permission from Ref. [85], © The Author(s) 2025.

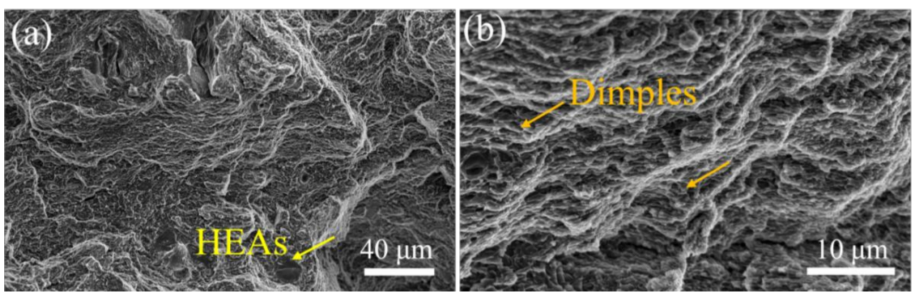

Fig. 15 Fracture surface of (TiB_2 + $AlCoCrFeNi_{2.1}$)/AlSi10Mg with 2 wt% $AlCoCrFeNi_{2.1}$. Reproduced with permission from Ref. [85], © The Author(s) 2025.

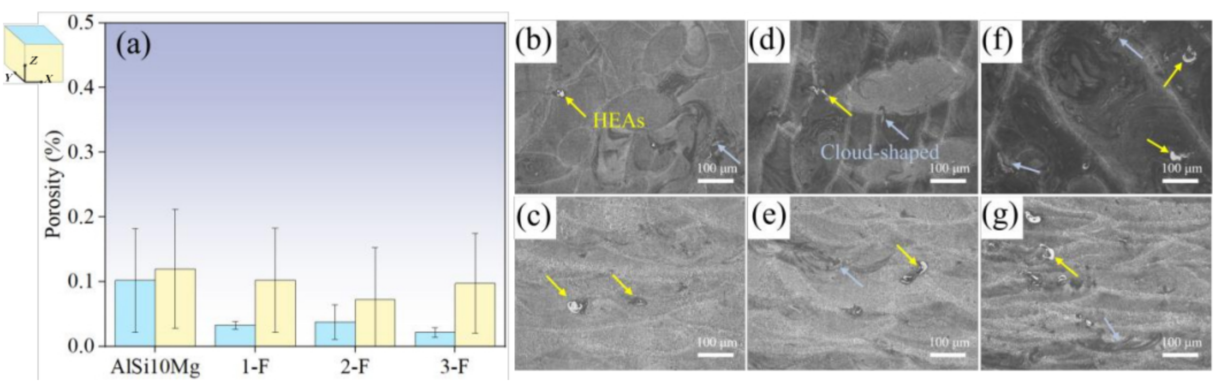

Fig. 16 Pore volume analysis of FeCoCrNi/AlSi10Mg composite materials. Reproduced with permission from Ref. [85], © The Author(s) 2025.

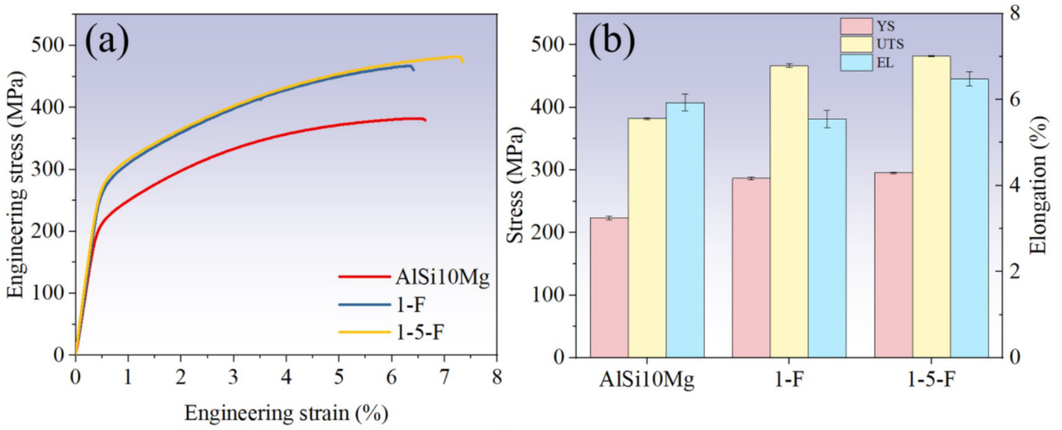

Fig. 17 Tensile properties of (FeCoCrNi + TiB_2)/AlSi10Mg composite materials. Reproduced with permission from Ref. [85], © The Author(s) 2025.

plasticity. This is primarily attributed to the excellent deformation capability of HEAs, enabling them to share load-bearing responsibilities with the matrix. Clearly, different HEAs exhibit distinct effects on composites, and HEAs processed via LPBF still follow the general rule that added reinforcements reduce material ductility. A small number of ceramic particles can mitigate the issue of reduced plasticity, enabling synergistic strengthening of both strength and percentage elongation in the composite material. Although the improvement in plasticity is not particularly significant, it represents an undeniable step forward. In-depth investigation into the interaction mechanisms between HEAs and aluminum alloys may enable better prediction of optimal HEAs for specific target alloys, potentially leading to significant simultaneous enhancement of strength, ductility, and percentage elongation in AMCs.

5 Summary and outlook

This review outlines the research background of AMCs fabricated via LPBF, as well as the performance characteristics and reinforcing effects of HEAs, and focuses on the current status and latest progress in LPBF-formed HEA/AlSi10Mg composites. Currently, aluminum alloys suitable for LPBF are primarily Al–Si alloys, especially AlSi10Mg, while forming challenges for other high-strength aluminum alloys remain to be addressed. AlSi10Mg exhibits favorable comprehensive properties when processed via LPBF. Incorporating HEAs significantly enhances both strength and ductility in the composite material, challenging the conventional strengthening design paradigm that prioritizes strength at the expense of ductility. Micron-sized HEAs act as nucleating agents to refine the grain size, while the fine secondary phases formed at grain boundaries through slow diffusion further contribute to grain refinement and dispersion strengthening. Although HEAs remain partially unmelted during forming under optimal process parameters for aluminum alloy, they exhibit strong bonding strength with the aluminum matrix. The high-strength HEAs possess inherent plasticity, and their robust interfacial bonding prevents premature failure at the interface during deformation. Consequently, the composite material achieves enhanced strength without a significant compromise in plasticity. Nevertheless, HEAs cannot entirely overcome the major issue of reinforcement phases sacrificing material ductility. This may stem from reactions between HEAs and the aluminum matrix, which inevitably produce some intermetallic compounds that increase composite brittleness. The addition of HEAs also influences melt pool evolution, inevitably introducing some porosity defects. While HEAs alone provide considerable strengthening effects, blending them with appropriate ceramic particles allows leveraging the advantages of both while mitigating some negative impacts of ceramic reinforcements, achieving simultaneous enhancement of strength and percentage elongation in composite materials. According to the current research, forming HEA-reinforced AMCs via LPBF does not resolve the issue of high internal stresses inherent to the LPBF process itself, and subsequent heat treatment is still required to relieve these stresses. It is important to note that the internal mechanisms of HEAs are complex. When incorporated into aluminum alloys, they may introduce not only traditional strengthening mechanisms such as grain refinement and secondary strengthening but also more intricate underlying effects that require further analytical research. Furthermore, current LPBF-based preparation methods for this reinforcement technique primarily exploit laser melting properties, specifically the grain refinement and strength enhancement achieved through controlled rapid heating and cooling, without fully leveraging additive manufacturing's unique advantages over traditional processes, such as structural design capabilities. In addition, since internal defects in materials formed via LPBF are quite pronounced, it is necessary to minimize these defects by optimizing the fabrication environment, process parameters, and even structural design to achieve the theoretical level of compatibility between HEAs and aluminum alloys under LPBF conditions to the greatest extent possible. Future research that thoroughly analyzes the strengthening mechanisms of HEAs in AMCs and integrates design concepts suited to LPBF additive manufacturing into the study of HEA-reinforced AMCs could make the process more controllable and predictable. This approach holds promise for simultaneous improvement in strength and plasticity as well as mitigation of internal stress, paving the way for widespread adoption and a new phase of development.

Acknowledgements

We acknowledge the financial support of the State Key Laboratory of Solidification Processing in NPU (No. SKLSP202516), the Guangdong Provincial Ordinary University Characteristic Innovation Project (No. 2023KTSCX265), the Guangdong Provincial Ordinary University Key Field Special Project (No. 2024ZDZX3108), Yichun Science and Technology Plan Project (No. 2024ZDYFZX02), and the Major Science and Technology Project of Yunfu City (No. 2024090401).

Availability of data and materials

The data that support the findings of this study are available from the corresponding author upon reasonable request.

Competing interest

The authors have no competing interests to declare that are relevant to the content of this article.

References

[1] Rong GF, Xin WJ, Zhou MX, *et al*. Exploring microstructure, wear resistance, and electrochemical properties of AlSi10Mg alloy fabricated using spark plasma sintering. *Materials-Basel* 2023, **16**: 7394.

[2] Cheng W, Ma XQ, Zhang JL, *et al*. Stability of weld pool and elimination of weld defects in aluminum alloy plasma arc keyhole welding at continuously varying positions. *Materials-Basel* 2021, **14**: 5898.

[3] Ashkenazi D. How aluminum changed the world: A metallurgical revolution through technological and cultural perspectives. *Technol Forecast Soc* 2019, **143**: 101–113.

[4] Cardinale AM, Macciò D, Luciano G, *et al*. Thermal and corrosion behavior of as cast AlSi alloys with rare earth elements. *J Alloys Compd* 2017, **695**: 2180–2189.

[5] Kasprzak W, Amirkhiz BS, Niewczas M. Structure and properties of cast Al–Si based alloy with Zr–V–Ti additions and its evaluation of high temperature performance. *J Alloys Compd* 2014, **595**: 67–79.

[6] Mehta A, Zhou L, Huynh T, *et al*. Additive manufacturing and mechanical properties of the dense and crack free Zr-modified aluminum alloy 6061 fabricated by the laser-powder bed fusion. *Addit Manuf* 2021, **41**: 101966.

[7] Zheng KL, Wei XS, Yan B, *et al*. Ceramic waste SiC particle-reinforced Al matrix composite brake materials with a high friction coefficient. *Wear* 2020, **458**: 203424.

[8] Wu SY, Chen B. Surface coatings of reinforcement phases in magnesium matrix composites: A review. *Materials* 2023, **16**: 7560.

[9] Spierings AB, Dawson K, Heeling T, *et al*. Microstructural features of Sc- and Zr-modified Al–Mg alloys processed by selective laser melting. *Mater Design* 2017, **115**: 52–63.

[10] Zhang H, Zhu HH, Nie XJ, *et al*. Effect of Zirconium addition on crack, microstructure and mechanical behavior of selective laser melted Al–Cu–Mg alloy. *Scripta Mater* 2017, **134**: 6–10.

[11] Wu JY, Yang HH, Lu GJ, *et al*. Microstructure and molten pool morphology of $TiB_2/AlSi_7Mg$ composites fabricated by infrared-blue hybrid laser powder bed fusion. *Heliyon* 2024, **10**: 25196.

[12] Li JJ, Yu WB, Sun ZY, *et al*. Influence of introducing Zr, Ti, Nb and Ce elements on externally solidified crystals and mechanical properties of high-pressure die-casting Al–Si alloy. *Int J Min Met Mater* 2025, **32**: 147–153.

[13] Sun JR, Dong BX, Yang HY, *et al*. The role of lithium in the aging precipitation process of Al–Zn–Mg–Cu alloys and its effect on the properties. *Materials* 2023, **16**: 4750.

[14] Yan A, Chen GX, Ying HQ, *et al*. High-entropy alloy activating laves-phase network for multi-component metallic coatings with high hardness. *Nanomaterials-Basel* 2024, **14**: 1016.

[15] Zhao ZY, Bai PK, Misra RDK, *et al*. AlSi10Mg alloy nanocomposites reinforced with aluminum-coated graphene: Selective laser melting, interfacial microstructure and property analysis. *J Alloys Compd* 2019, **792**: 203–214.

[16] An DY, Xiao Y, Yu JS, *et al*. The role of dislocation type in the thermal stability of cellular structures in additively manufactured austenitic stainless steel. *Adv Sci* 2024, **11**: 2402962.

[17] Nie JF, Chen YY, Song L, *et al*. Enhancing strength and ductility of Al-matrix composite via a dual-heterostructure strategy. *Int J Plasticity* 2023, **171**: 103825.

[18] Qu ML, Guo QL, Escano LI, *et al*. Controlling process instability for defect lean metal additive manufacturing. *Nat Commun* 2022, **13**: 1079.

[19] Wang XY, Lu QH, Zhang PL, *et al*. A review on the simulation of selective laser melting AlSi10Mg. *Opt Laser Technol* 2024, **174**: 110500.

[20] Liu G, Zhang XF, Chen XL, *et al*. Additive manufacturing of structural materials. *Mater Sci Eng R Rep* 2021, **145**: 100596.

[21] Yan Q, Song B, Shi YS. Comparative study of performance comparison of AlSi10Mg alloy prepared by selective laser melting and casting. *J Mater Sci Technol* 2020, **41**: 199–208.

[22] Hojjatzadeh SMH, Parab ND, Yan WT, *et al*. Pore elimination mechanisms during 3D printing of metals. *Nat Commun* 2019, **10**: 3088.

[23] Li XF, Yi DH, Wu XY, *et al*. Effect of construction angles on microstructure and mechanical properties of AlSi10Mg alloy fabricated by selective laser melting. *J Alloys Compd* 2021, **881**: 160459.

[24] Feng Z, Tan H, Fang YB, *et al*. Selective laser melting of TiB_2/AlSi10Mg composite: Processability, microstructure and fracture behavior. *J Mater Process Tech* 2022, **299**: 117386.

[25] Li C, Zhang WX, Yang HO, *et al*. Microstructural origin of high strength and high strain hardening capability of a laser powder bed fused AlSi10Mg alloy. *J Mater Sci Technol* 2024, **197**: 194–206.

[26] Li Z, Sui S, Ma X, *et al*. High deposition rate powder- and wire-based laser directed energy deposition of metallic materials: A review. *Int J Mach Tool Manu* 2022, **181**: 103942.

[27] Huangfu BH, Liu YJ, Liu XC, *et al*. Anisotropy of additively manufactured metallic materials. *Materials-Basel* 2024, **17**: 3653.

[28] Wu J, Wang XQ, Wang W, *et al*. Microstructure and strength of selectively laser melted AlSi10Mg. *Acta Mater* 2016, **117**: 311–320.

[29] Patidar S, Tiwari JK, Das A, *et al*. Study on microstructure and tribological behavior of additively manufactured graphene/AlSi10Mg composite. *J Mater Eng Perform* 2024, **33**: 12503–12516.

[30] Uzan NE, Ramati S, Shneck R, *et al*. On the effect of shot-peening on fatigue resistance of AlSi10Mg specimens fabricated by additive manufacturing using selective laser melting (AM-SLM). *Addit Manuf* 2018, **21**: 458–464.

[31] Tan QY, Chang HW, Liang GF, *et al*. High-performance plain carbon steels obtained through 3D-printing. *Nat Commun* 2024, **15**: 10077.

[32] Zheng Y, Xiong RZ, *et al*. Laser melting deposition of in-situ (TiB+TiC) hybrid reinforced TC4 composites: Preparation, microstructure and room/high-temperature corrosion behaviour. *J Mater Sci Technol* 2025, **228**: 137–154.

[33] Xiu ZY, Ju BY, Liu SY, *et al*. Spark plasma sintering of AlN/Al functionally graded materials. *Materials-Basel* 2021, **14**: 4893.

[34] Li XF, Feng YH, Liu B, *et al*. Influence of NbC particles on microstructure and mechanical properties of AlCoCrFeNi high-entropy alloy coatings prepared by laser cladding. *J Alloys Compd* 2019, **788**: 485–494.

[35] Pickering EJ, Jones NG. High-entropy alloys: A critical assessment of their founding principles and future prospects. *Int Mater Rev* 2016, **61**: 183–202.

[36] Pfeiffer OP, Liu HH, Montanelli L, *et al*. Aluminum alloy compositions and properties extracted from a corpus of scientific manuscripts and US patents. *Sci Data* 2022, **9**: 128.

[37] Rometsch PA, Zhu YM, Wu XH, *et al*. Review of high-strength aluminium alloys for additive manufacturing by laser powder bed fusion. *Mater Design* 2022, **219**: 110779.

[38] Kenevisi MS, Yu YF, Lin F. A review on additive manufacturing of Al–Cu (2xxx) aluminium alloys, processes and defects. *Mater Sci Tech Ser* 2021, **37**: 805–829.

[39] Azarniya A, Taheri AK, Taheri KK. Recent advances in ageing of 7xxx series aluminum alloys: A physical metallurgy perspective. *J Alloys Compd* 2019, **781**: 945–983.

[40] Minasyan T, Hussainova I. Laser powder-bed fusion of ceramic particulate reinforced aluminum alloys: A review. *Materials-Basel* 2022, **15**: 2467.

[41] Mair P, Goettgens VS, Rainer T, *et al*. Laser powder bed fusion of nano-CaB_6 decorated 2024 aluminum alloy. *J Alloys Compd* 2021, **863**: 158714.

[42] Peng ZX, Xu W, Liu Y, *et al*. Anisotropy evaluation and defect detection on laser power bed fusion 316L stainless steel. *Micromachines-Basel* 2023, **14**: 1206.

[43] Revilla R, Verkens D, Rubben T, *et al.* Corrosion and corrosion protection of additively manufactured aluminium alloys—A critical review. *Materials-Basel* 2020, **13**: 4804.
[44] Zhang H, Zhu HH, Qi T, *et al.* Selective laser melting of high strength Al–Cu–Mg alloys: Processing, microstructure and mechanical properties. *Mater Sci Eng A-Struct* 2016, **656**: 47–54.
[45] Tan QY, Liu YG, Fan ZQ, *et al.* Effect of processing parameters on the densification of an additively manufactured 2024 Al alloy. *J Mater Sci Technol* 2020, **58**: 34–45.
[46] Pekok MA, Setchi R, Ryan M, *et al.* Effect of process parameters on the microstructure and mechanical properties of AA2024 fabricated using selective laser melting. *Int J Adv Manuf Tech* 2021, **112**: 175–192.
[47] Tucho WM, Lysne VH, Austbø H, *et al.* Investigation of effects of process parameters on microstructure and hardness of SLM manufactured SS316L. *J Alloys Compd* 2018, **740**: 910–925.
[48] Lv Y, Liu Z, Zhang H, *et al.* Process optimization and defect suppression of Inconel 718 superalloy fabricated by laser powder bed fusion via response surface methodology. *J Mater Res Technol* 2023, **24**: 10163–10176.
[49] Dong ZC, Xu MC, Guo HW, *et al.* Microstructural evolution and characterization of $AlSi_{10}Mg$ alloy manufactured by selective laser melting. *J Mater Res Technol* 2022, **17**: 2343–2354.
[50] Yao S, Wang JJ, Li M, *et al.* LPBF-formed 2024Al alloys: Process, microstructure, properties, and thermal cracking behavior. *Metals-Basel* 2023, **13**: 268.
[51] Wen XL, Wang QZ, Mu Q, *et al.* Laser solid forming additive manufacturing TiB_2 reinforced 2024 Al composite: Microstructure and mechanical properties. *Mater Sci Eng A-Struct* 2019, **745**: 319–325.
[52] Jia QB, Zhang F, Rometsch P, *et al.* Precipitation kinetics, microstructure evolution and mechanical behavior of a developed Al–Mn–Sc alloy fabricated by selective laser melting. *Acta Mater* 2020, **193**: 239–251.
[53] Croteau JR, Griffiths S, Rossell MD, *et al.* Microstructure and mechanical properties of Al–Mg–Zr alloys processed by selective laser melting. *Acta Mater* 2018, **153**: 35–44.
[54] Yin ZM, Pan QL, Zhang YH, *et al.* Effect of minor Sc and Zr on the microstructure and mechanical properties of Al–Mg based alloys. *Mater Sci Eng A-Struct* 2000, **280**: 151–155.
[55] Scudino S, Liu G, Prashanth KG, *et al.* Mechanical properties of Al-based metal matrix composites reinforced with Zr-based glassy particles produced by powder metallurgy. *Acta Mater* 2009, **57**: 2029–2039.
[56] Li XP, Ji G, Chen Z, *et al.* Selective laser melting of nano-TiB_2 decorated AlSi10Mg alloy with high fracture strength and ductility. *Acta Mater* 2017, **129**: 183–193.
[57] Onawale OT, Cobbinah PV, Nzeukou RA, *et al.* Synthesis route, microstructural evolution, and mechanical property relationship of high-entropy alloys (HEAs): A review. *Materials-Basel* 2021, **14**: 3065.
[58] Martin JH, Yahata BD, Hundley JM, *et al.* 3D printing of high-strength aluminium alloys. *Nature* 2017, **549**: 365–369.
[59] Yang T, Liu TT, Liao WH, *et al.* Laser powder bed fusion of AlSi10Mg: Influence of energy intensities on spatter and porosity evolution, microstructure and mechanical properties. *J Alloys Compd* 2020, **849**: 156300.
[60] Guo QL, Zhao C, Qu ML, *et al.* *In situ* characterization and quantification of melt pool variation under constant input energy density in laser powder bed fusion additive manufacturing process. *Addit Manuf* 2019, **28**: 600–609.
[61] Liu H, Liu J, Chen PJ, *et al.* Microstructure and high temperature wear behaviour of *in-situ* TiC reinforced AlCoCrFeNi-based high-entropy alloy composite coatings fabricated by laser cladding. *Opt Laser Technol* 2019, **118**: 140–150.
[62] Chen B, Moon SK, Yao X, *et al.* Strength and strain hardening of a selective laser melted AlSi10Mg alloy. *Scripta Mater* 2017, **141**: 45–49.
[63] Lei ZF, Liu XJ, Wu Y, *et al.* Enhanced strength and ductility in a high-entropy alloy via ordered oxygen complexes. *Nature* 2018, **563**: 546–550.
[64] Li SY, Luo T, Chao ZL, *et al.* A review of dynamic mechanical behavior and the constitutive models of aluminum matrix composites. *Materials-Basel* 2024, **17**: 1879.
[65] Chen Y, Jian ZY, Ren YM, *et al.* Influence of TiB_2 volume fraction on SiC_p/AlSi10Mg composites by LPBF: Microstructure, mechanical, and physical properties. *J Mater Res Technol* 2023, **23**: 3697–3710.
[66] Fan ZH, Yan XC, Fu ZY, *et al.* *In situ* formation of D022-Al_3Ti during selective laser melting of nano-TiC/$AlSi_{10}Mg$ alloy prepared by electrostatic self-assembly. *Vacuum* 2021, **188**: 110179.
[67] Li YL, Feng HK, Cao FR, *et al.* Effect of high density ultrasonic on the microstructure and refining property of Al–5Ti–0.25C grain refiner alloy. *Mater Sci Eng A-Struct* 2008, **487**: 518–523.
[68] Yang HY, Wang Z, Chen LY, *et al.* Interface formation and bonding control in high-volume-fraction (TiC + TiB_2)/Al composites and their roles in enhancing properties. *Compos Part B-Eng* 2021, **209**: 108605.
[69] Han CJ, Babicheva R, Chua JDQ, *et al.* Microstructure and mechanical properties of (TiB+TiC)/Ti composites fabricated *in situ* via selective laser melting of Ti and B_4C powders. *Addit Manuf* 2020, **36**: 101466.
[70] Li W, Yang Y, Liu J, *et al.* Enhanced nanohardness and new insights into texture evolution and phase transformation of TiAl/TiB_2 *in situ* metal matrix composites prepared via selective laser melting. *Acta Mater* 2017, **136**: 90–104.
[71] Lee DH, Jung JY, Lee KH, *et al.* Distinct effects of *in situ* and *ex-situ* hydrogen charging methods on the mechanical behavior of CoCrFeNi high-entropy alloy fabricated by laser powder bed fusion. *J Alloys Compd* 2023, **940**: 168858.
[72] Cantor B, Chang ITH, Knight P, *et al.* Microstructural development in equiatomic multicomponent alloys. *Mater Sci Eng A-Struct* 2004, **375**: 213–218.
[73] Yeh JW, Chen SK, Lin SJ, *et al.* Nanostructured high-entropy alloys with multiple principal elements: Novel alloy design concepts and outcomes. *Adv Eng Mater* 2004, **6**: 299–303.
[74] George EP, Curtin WA, Tasan CC. High-entropy alloys: A focused review of mechanical properties and deformation mechanisms. *Acta Mater* 2020, **188**: 435–474.
[75] Toda-Caraballo I, Rivera-Díaz-del-Castillo PEJ. Modelling solid solution hardening in high entropy alloys. *Acta Mater* 2015, **85**: 14–23.
[76] Kumar A, Singh A, Suhane A. Mechanically alloyed high entropy alloys: Existing challenges and opportunities. *J Mater Res Technol* 2022, **17**: 2431–2456.
[77] Jung C, Nam S, Son H, *et al.* Simultaneous enhancement of strength and ductility of Al matrix composites enabled by submicron-sized high-entropy alloy phases. *J Mater Res Technol* 2024, **33**: 1470–1478.
[78] Gao CQ, Wang QB, Wei MY, *et al.* Effects of reinforcement volume fraction on mechanical properties and microstructures of 7075 Al matrix composites reinforced by FeCoCrNiAl high-entropy alloy particles. *Metals-Basel* 2022, **12**: 851.
[79] Huang XJ, Zhang JY, Miao JS, *et al.* On the interactions between molten aluminum and high entropy alloy particles during aluminum matrix composite processing. *J Alloys Compd* 2022, **895**: 162712.
[80] Yang X, Liang ZM, Wang LW, *et al.* Interface structure and tensile behavior of high entropy alloy particles reinforced Al matrix composites by spark plasma sintering. *Mater Sci Eng A-Struct* 2022, **860**: 144273.
[81] Liu YZ, Chen J, Wang XH, *et al.* Significantly improving strength and plasticity of Al-based composites by *in situ* formed AlCoCrFeNi core-shell structure. *J Mater Res Technol* 2021, **15**: 4117–4129.
[82] Zhu DZ, Chen TT, Jin XQ, *et al.* Quasi-static and dynamic deformation of aluminum matrix composites reinforced by core-shell $Al_{35}Ti_{15}Cu_{10}Mn_{20}Cr20$ high-entropy alloy particulates. *J Mater Res Technol* 2024, **30**: 1009–1019.

[83] Yang C, Ren C, Jia YF, *et al*. A machine learning-based alloy design system to facilitate the rational design of high entropy alloys with enhanced hardness. *Acta Mater* 2022, **222**: 117431.

[84] Yuan PP, Gu DD. Molten pool behaviour and its physical mechanism during selective laser melting of TiC/AlSi10Mg nanocomposites: Simulation and experiments. *J Phys D Appl Phys* 2015, **48**: 035303.

[85] Chen SY. Microstructure and properties of high-entropy alloys reinforced AlSi10Mg composites fabricated by selective laser melting. Master's Thesis. Guangzhou (China): South China University of Technology, 2025.

[86] Li PB, Peng KX, Wu BT, *et al*. Mechanical properties of Al–Si matrix composites synergistically reinforced by high-entropy alloy and SiC nanoparticles. *J Alloys Compd* 2023, **939**: 168762.

[87] Wang HM, Su WX, Liu JQ, *et al*. Microstructure and properties of FeCoNiCrMn and Al_2O_3 hybrid particle-reinforced aluminum matrix composites fabricated by microwave sintering. *J Mater Res Technol* 2023, **24**: 8618–8634.

[88] Luo KG, Xiong HQ, Zhang Y, *et al*. AA1050 metal matrix composites reinforced by high-entropy alloy particles via stir casting and subsequent rolling. *J Alloys Compd* 2022, **893**: 162370.

[89] Huan CB, He YQ, Su QH, *et al*. Properties of $AlFeNiCrCoTi_{0.5}$ high-entropy alloy particle-reinforced 6061 Al composites prepared by extrusion. *Metals-Basel* 2022, **12**: 1325.

[90] Wang P, Qi JF, Chen ZW, *et al*. Microstructure and mechanical properties of novel high-entropy alloy particle reinforced aluminum matrix composites fabricated by selective laser melting. *J Alloys Compd* 2021, **868**: 159197.